TITLE: Lack of MeCP2 leads to region-specific increase of doublecortin in the olfactory system

AUTHORS: Elena Martínez-Rodríguez[1], Ana Martín-Sánchez[2§], Simona Coviello[3], Cristina Foiani[1], Emre Kul[4], Oliver Stork[4], Fernando Martínez-García[2], Juan Nacher[3], Enrique Lanuza[1], Mónica Santos[4*], Carmen Agustín-Pavón[1*]

1. Unitat Mixta d'Investigació Neuroanatomia Funcional, Departament de Biologia Cel·lular, Funcional i Antropologia Física, Universitat de València (Spain).
2. Unitat Mixta d'Investigació Neuroanatomia Funcional, Unitat Predepartamental de Medicina, Universitat Jaume I, Castelló (Spain).
3. Neurobiology Unit, Departament de Biologia Cel·lular, Funcional i Antropologia Física, Interdisciplinary Research Structure for Biotechnology and Biomedicine (BIOTECMED), Universitat de Valencia (Spain); CIBERSAM: Spanish National Network for Research in Mental Health (Spain); Fundación Investigación Hospital Clínico de Valencia, INCLIVA, Valencia (Spain).
4. Department of Genetics and Molecular Neurobiology, Institute of Biology, and Center for Behavioral Sciences, Otto-von-Guericke University, Magdeburg (Germany)

[§] Current adress: Departament de Ciències Experimentals i de la Salut, Grup de Recerca en Neurobiologia del Comportament (GReNeC-NeuroBio), Institut Hospital del Mar d'Investigacions Mèdiques (IMIM), Universitat Pompeu Fabra, Barcelona (Spain)

* Correspondence:

Carmen Agustín-Pavón

ORCID ID: 0000-0002-6725-6954

Departament de Biologia Cel·lular, Biologia Funcional i Antropologia Física, Universitat de València

Av. Vicent Andrés Estellés, s/n 46100 Burjassot, Spain

Email: pavon@uv.es

Mónica Santos

ORCID ID: 0000-0003-3229-8270

Institute of Biology, Otto-von-Guericke University, Magdeburg (Germany)

Email: monicapsantos@hotmail.com

ACKNOWLEDGEMENTS

Authors are indebted to Marta Igual, Adriana Gregory-Flores and Rylie Frese for their help in cell counting, and to Dr Guillermo Ayala for statistical advice.

ABSTRACT

The protein doublecortin is mainly expressed in migrating neuroblasts and immature neurons. The X-linked gene *MECP2,* associated to several neurodevelopmental disorders such as Rett Syndrome, encodes the protein methyl-CpG-binding protein 2 (MeCP2), a regulatory protein that has been implicated in neuronal maturation and refinement of olfactory circuits. Here we explored doublecortin immunoreactivity in the brain of young-adult female *Mecp2*-heterozygous and male *Mecp2*-null mice and their wild-type littermates. The distribution of doublecortin-immunorective somata in neurogenic brain regions was consistent with previous reports in rodents, and no qualitative differences were found between genotypes or sexes. Quantitatively, we found a significant increase in doublecortin cell density in in the piriform cortex of *Mecp2*-null males as compared to WT littermates. A similar increase was seen in a newly-identified population of doublecortin cells in the olfactory tubercle. In these olfactory structures, however, the percentage of doublecortin immature neurons that also expressed NeuN was not different between genotypes. By contrast, we found no significant differences between genotypes in doublecortin-immunorectivity in the olfactory bulbs. Nonetheless, in the periglomerular layer of *Mecp2*-null males we observed a specific decrease of immature neurons co-expressing doublecortin and NeuN. Overall, no differences were evident between *Mecp2*-heterozygous and WT females. Also, no differences could be detected between genotypes in the density of doublecortin-immunoreactive cells in the hippocampus or striatum of either males or females. Our results suggest that MeCP2 is involved in neuronal maturation in a region-dependent manner.

Keywords: Adult non-proliferative neurogenesis; Neuronal maturation; Olfactory tubercle; Plasticity; Piriform cortex; Rett syndrome

ABBREVIATIONS

Aca Anterior Commissure

AcbC Nucleus Accumbens Core

AOB Accessory Olfactory Bulb

AOL Anterior Olfactory Nucleus, Lateral

AOM Anterior Olfactory Nucleus, Medial

AOV Anterior Olfactory Nucleus, Ventral

CC Corpus Callosum

CPu Caudatus Putamen

DG Dentate Gyrus

dSt Dorsal Striatum

Gl Glomerular cell layer of the Olfactory Bulb

Gr Granular cell layer of the Olfactory Bulb

GrDG Granular layer of the Dentate Gyrus

LV Lateral Ventricle

Mi Mitral cell layer of the Olfactory Bulb

Mol Molecular layer of the Dentate Gyrus

OB Olfactory Bulbs

Pir Piriform Cortex

PGl Periglomerular layer of the Olfactory Bulb

PoDG Polymorphic-oriens later of the Dentate Gyrus

RMS Rostral Migratory Stream

SVZ Subventricular Zone

Tu Olfactory Tubercle

vSt Ventral Striatum

INTRODUCTION

Doublecortin (DCX) is a microtubule-associated protein expressed in migrating neuroblasts and differentiating neurons (Gleeson et al. 1998; Francis et al. 1999), and hence it is frequently used as a neurogenic marker (Saaltink et al. 2012). In the adult rodent brain, DCX expression is restricted to the neurogenic areas of the subventricular zone (SVZ), rostral migratory stream (RMS), olfactory bulb (OB), and dentate gyrus (DG) of the hippocampus (Nacher et al. 2002; Saaltink et al. 2012). In addition, some DCX-immunoreactive (DCX-ir) cells with neuronal morphology are found in the striatum next to the SVZ (Nacher et al. 2002). Finally, there is an interesting population of DCX-ir neurons in layer II of the piriform cortex (Pir), which is mostly generated during embryonic development, persist in adulthood and decline with aging (Gómez-Climent et al. 2008; Rubio et al. 2016). These cells have been recently shown to mature and integrate as glutamatergic neurons (Rotheneichner et al. 2018). In fact, in rodents and in other mammalian species the DCX-ir cells express the transcription factor Tbr-1 (Luzzati et al. 2009), which is characteristic of the pallial glutamatergic projection neurons (Guillemot et al. 2006). They may constitute a source of neural plasticity, which may contribute to some forms of olfactory learning (but see Gómez-Climent et al. 2011).

The gene *MECP2*, located at chromosome X, encodes the methyl-CpG-binding protein 2 (MeCP2), which has been suggested to play an important role in neuronal differentiation and maturation (Kishi and Macklis 2004), roles that have been investigated in the olfactory system (Cohen et al. 2003; Ronnett et al. 2003; Matarazzo et al. 2004). Initially described as a transcriptional repressor (Nan et al. 1993, 1997), MeCP2 is currently known as a modulator of gene expression by interacting with different partners (Lombardi et al. 2015). Mutations in *MECP2* have been associated to several neurodevelopmental disorders causing intellectual disability and autism (Gonzales and LaSalle 2010), of which Rett syndrome (RTT) is the most representative (Amir et al. 1999). Girls affected with this syndrome are born apparently healthy. From 6-18 months of age they start to show overt developmental problems, such as regression of the acquired skills, autonomic and motor impairment, repetitive behaviours, intellectual disability and loss of speech (Hagberg 2002). On the other hand, boys with classic *MECP2* mutations generally suffer from severe neonatal encephalopathy and die before the age of 1 year (reviewed in Santos et al. 2009).

Murine models in which *Mecp2* has been knocked out (KO) (Chen et al. 2001; Guy et al. 2001) provide a valuable tool to investigate the role of MeCP2 in the development and organization of the nervous system. Male *Mecp2* KO mice show overt RTT phenotype by 6-8 weeks of age and premature death

around 60 days of age, whereas in heterozygous (HET) females phenotype onset occurs by three months of age (Guy et al. 2001). The approximate correspondence in real time between RTT human and mouse phenotype argues in favour of no defects in developmental neurogenesis, but rather an effect in maintenance of neuronal functionality (Guy et al. 2001). Accordingly, in rodent and human brains, the levels of MeCP2 protein are faint during brain embryonic development and reach the highest levels in more mature structures (Shahbazian et al. 2002; Cassel et al. 2004; Mullaney et al. 2004). In addition, in 9 weeks old mice virtually all MeCP2-ir cells co-express NeuN, hence should be considered as mature neurons (Kishi and Macklis 2004).

In this framework, we sought to investigate the effect of MeCP2 deficiency in the distribution and density of DCX-ir neurons in the young adult mouse brain, focusing on the olfactory system. To do so, we performed an immunohistochemical detection of DCX in young adult female HET (*Mecp2*$^{+/-}$) and male KO (*Mecp2*$^{y/-}$) and their male and female WT littermates. Given the previously suggested role of MeCP2 in neuronal maturation, we hypothesised that *Mecp2*-deficient animals may display an increased density of immature neurons, and hence an increase in DCX-ir with respect to their WT controls.

MATERIALS AND METHODS

Animals

For these experiments, we used 30 *Mecp2*$^{tm1.1Bird/J}$ mice (Guy et al. 2001) purchased at The Jackson Lab and their WT siblings. Mice were used at age 8 weeks old (female *Mecp2*$^{+/-}$, n=5; male *Mecp2*$^{y/-}$, n=9; female WT, n=6; male WT, n=10). Mice were housed in standard laboratory cages in groups of 2-5 animals, with controlled humidity and temperature (22ºC), a 12:12-h inverted light/dark cycle, and water and food available *ad libitum*. For genotyping, we obtained tail tips at weaning and after DNA extraction we applied the protocol supplied for this strain by the Jackson Laboratory. The protocols were approved by the local veterinary office and carried out in strict accordance with EU directive 2010/63/EU and the German law.

Perfusion and histology

Animals were deeply anaesthetized using a mixture of ketamine (75 mg/Kg) and medetomidine (1 mg/Kg) and transcardially perfused with saline solution followed by 4% paraformaldehyde in 0.1M phosphate buffer, pH 7.4. Brains were carefully removed from the skull, postfixed in the same fixative overnight and passed to 30% sucrose in 0.01M phosphate buffered saline (PBS), pH 7.6) until they sank. The brains were then frozen and cut in five series of 40-µm-thick coronal sections with a cryostat. Free-floating sections

were collected in five parallel series and frozen in phosphate buffered 30% sucrose (0.1 M, pH 7.4) for future processing.

Doublecortin immunohistochemistry

We first obtained permanent immunostained preparations for DCX in one out of the five parallel series in all the females (WT, n=6, Mecp2$^{+/-}$=5) and a subset of males (WT, n=7; *Mecp2*$^{y/-}$, n=5), using the indirect avidin–biotin complex/DAB-staining procedure. In brief, brain slices were first incubated with 1% H_2O_2 in 0.05M tris-buffered saline (TBS, 0.9% NaCl in TB) for 30 minutes at room temperature (RT) to block endogenous peroxidase activity. Subsequently, sections were incubated with 2% normal horse serum (NHS) and 0.3% Triton-X100 in 0.05M TBS pH 7.4 for one hour at RT, to block nonspecific binding. Brain slices were then incubated over night at 4 ºC with a goat primary antibody anti-DCX (Santa Cruz Biotechnology, Inc) diluted 1:500 in 0.05M TBS pH 7.4, with 2% NHS and 0.3% Triton-X100. The next day, sections were incubated for two hours at RT with biotinylated horse anti-Goat-IgG secondary antibody (Vector) diluted 1:200 in the same buffer. Afterwards, sections were incubated for 90 minutes at RT in avidin-biotin-peroxidase complex (ABC; Vector) in TBS with 0.3% Triton-X100. Sections were thoroughly washed in TBS (3x 10 min) between each step. To reveal peroxidase activity, sections were incubated for five minutes in 3,3'-diaminobenzidine (DAB)-SigmaFAST (Sigma) in TB. Sections were mounted using 0.2% gelatine in TB, dehydrated with alcohol, cleared with xylol and cover-slipped with Entellan.

DAPI labelling

We obtained DAPI-labelled sections in one out of the five parallel series by incubating tissue for 45 seconds in 600nM DAPI (4',6-diamino-2-feniindol) at RT. Sections were then rinsed thoroughly in TB, mounted on gelatinized slides and cover-slipped with fluorescence mounting medium (Dako, Glosrup, Denmark).

Immunofluorescence for co-labelling of Doublecortin and NeuN

Since data on DAB-stained samples revealed some differences between genotypes in males, but not in female mice, we sought to further characterize the DCX-expressing population by obtaining a simultaneous labelling of DCX and NeuN in one out of the five parallel series from experimental males (WT, n=10; *Mecp2*$^{y/-}$, n=8). Cells co-expressing DCX and NeuN are refereed to as "transitioning neurons", since they are immature neurons transitioning to maturity. Briefly, brain slices were incubated with 1% sodium borohydride ($NaBH_4$) in 0.05M TBS for 30 minutes at RT to eliminate the endogenous fluorescence of the tissue. Next, nonspecific binding was blocked by incubating slices in with 4% Normal Donkey Serum (NDS) in 0.05 TBS and 0.3% Triton-X100 for 1 hour at RT. Subsequently, sections were incubated for two

nights at 4ºC with a mix of primary antibodies: mouse anti-NeuN IgG (Chemicon) diluted 1:2500 and goat anti-DCX IgG (Santa Cruz Biotechnology, Inc) diluted 1:250, in 0.05M TBS pH 7.6 with 2% NDS and 0.3% Triton-X100. Afterwards, brain slices were incubated for 90 minutes at RT in darkness, with a mix of the two secondary antibodies, Alexa Fluor 488-conjugated Donkey anti-mouse IgG and Alexa Fluor 568-conjugated Donkey anti-goat IgG, both diluted 1:250 in 0.05M TBS pH 7.6 with 2% NDS and 0.3% Triton-X100. Sections were thoroughly rinsed between each step in TBS. Finally, sections were mounted in slides with 0.2% gelatine in TB, and cover-slipped with FluorSave TM Reagent.

Quantification of DCX-immunoreactive cells and double-labelled DCX/NeuN-immunofluorescent cells

For convenience, from now on we will use the abbreviation DCX-ir for samples stained with the ABC/DAB procedure, and DCX-if for samples labelled with immunofluorescence. We analysed DCX-ir and DCX/NeuN-if with a confocal microscope (Leica, TCS-SPE) and microscope equipped with both conventional light and fluorescence lamps (Leica Leitz DMRB), equipped with a digital camera (Leica DFC495) and software LAS v4.3 at *a priori* selected Bregma levels, according to Paxinos and Franklin mouse brain atlas (2012), (Table 1). For quantification of DCX-ir cells, we performed a pilot of counting in the Pir, carried out by three experimenters who were blind to the genotype and sex of the mice by using the Multipoint plugin of the Image-J image analysis software (NIH). Since no significant differences were found between measures taken by different experimenters, the number of DCX-ir cells was quantified by one researcher blinded to experimental groups. Cells in the dorsal and ventral striatum were quantified in the same way as the ones in the Pir, and cell density was calculated as number of cells per mm^2 of the ROI. In the olfactory tubercle (Tu) and DG, due to the low and high density of cells, respectively, counts were performed with a manual counter at higher magnification, and cell density is presented in number of cells per coronal section. For quantification of immunofluorescent labelling, we obtained images at the same Bregma levels (Table 1) with the 488 and 568 nm filters. Next, we merged the photos of both channels using Image-J, and quantified single DCX-if and double DCX/NeuN-if cells with the Multipoint plugin. In the OB, due to the high density of cells and fibres, we calculated the area fraction covered by DCX-ir in DAB-stained material by converting the image to greyscale by splitting the RGB image into the three channels and selecting the green channel -since it provides the better contrast for DAB staining-, and binarizing by establishing 90% of the grey histogram mode as a threshold level. We normalised these data by dividing the area fraction covered by DCX-ir elements in the OB by the area fraction covered by DCX-ir elements (mostly glial cells) in the anterior olfactory nucleus, and calculated the average area fraction of

all Bregma levels analysed, hence obtaining a single measure per animal. Finally, to quantify the immunofluorescence in the granular layer of the OB, we split the RGB image, selected the red channel, inverted the greyscale resulting image and measured the optical density.

Quantification of DAPI staining

We obtained photographs in the same levels of the Pir as described in Table 1 with the Leica Leitz DMRB microscope with excitation wavelength of 405 nm. DAPI-labelled nuclei were counted manually by a researcher who was blind to the sex and genotype of the animals with the multipoint plugin and the GRID tool of ImageJ. We counted DAPI-labelled neuronal-like, regularly-shaped nuclei of around 10 µm of diameter, in 12 squares of $3x10^3$ μm^2 in each slice.

Statistical Analyses

Data were analysed using the software IBM SPSS Statistics 22.0. First, we checked the data for normality (Kolmogorov-Smirnov's test) and homoscedasticity (Levene's test). Next, data were evaluated t-Student tests. Significance level was set at $p < 0.05$.

RESULTS

Distribution of DCX-ir cell bodies is not affected by sex or genotype

The distribution of DCX-ir somata in our DAB-stained samples was consistent with that previously described in the rat (Nacher et al. 2002) and mouse (Saaltink et al. 2012) brains. No differences in distribution were apparent between DAB-stained or fluorescence-labelled samples. Overall, we found abundant DCX-ir in the SVZ of the lateral ventricles (Figure 1A) and RMS (Figure 1D, D'; Figure 2A). Some of the cells next to SVZ were integrated in the striatal parenchyma both at the dorsomedial part of the striatum (dSt; Figure 1A, inset) and the ventral striatum (vSt; accumbens core and lateral septum) next to the ventral tip of the ventricle (Figure 1B, B'). Abundant DCX-ir neuronal somata were also present in the subgranular zone of the DG of the hippocampus (Figure 1C) and granular (Gr) and periglomerular (PGl) layers of the OB (Figure 1D, D'; Figure 2A, B), in the piriform cortex (Figure 1E, E'; Figure 2C) and dorsal and ventral endopiriform nuclei. Importantly, we discovered a previously unnoticed, to our knowledge, small population of DCX-ir cells in layer I of the Tu (Figure 1F, F', Figure 2D; Supplementary Information). These cells displayed abundant processes and sometimes were densely packed in groups of 5-10 cells, especially in the mutant animals (Figure 1F', Figure 2D). Since these DCX-expressing cells were quite scarce, and although further in-depth characterization of these cells is out of the scope of this paper, we sought to confirm their presence in another strain of mice (Supplementary Information). In FVB-

WT male mice, DCX-if cells in the Tu were present in similar numbers as in the WT littermates of *Mecp2*-mutants, derived from B6 strains (5.3±1.2 cells/section vs 6.17 cells/section±1.8, compare Supplementary Information and Table 2). Further, around 80% of these DCX-if cells co-expressed the polysialylated form of the neural cell adhesion molecule (PSA-NCAM), a plasticity marker described to co-locate with DCX in the Pir immature population of layer II (Rubio et al. 2016), and some of them co-expressed the neuronal nuclear antigen (NeuN), a neuronal marker (Supplementary Information). These data suggest that DCX-if cells in the Tu might be, although scarce, biologically significant, immature neurons.

DCX-ir cell density is increased in olfactory structures in Mecp2$^{y/-}$ male mice

We first quantified the density of DCX-ir in our DAB-stained material, and then confirmed some of the significant differences found, or their lack thereof, in our immunofluorescent samples. Area fraction covered by DCX-ir in the OB was not significantly different between females of both genotypes (t=-1.1, p=0.325, Table 2), or between *Mecp2*$^{y/-}$males and WT (t=-2.23, p=0.06, Table 2). Accordingly, in the samples labelled with immunofluorescence, we found no significant differences between *Mecp2*$^{y/-}$ and their WT littermates in optic density of DCX-if in the granular layer or in the number of DCX-if cells in the periglomerular cell layer (t=-0.75, p=0.46) (Table 2). Thus, globally, DCX expression in the OB seems not affected by lack or deficiency of MeCP2.

In the Pir of females, we found no significant differences between genotypes (t=-0.82, p=0.431, Table 2), but both DCX-ir and DCX-if cell density was significantly higher in the Pir of *Mecp2*$^{y/-}$ males than in their WT littermates (t=-4.20, p=0.002, and t=-2.80, p=0.013, respectively, Table 2).

Since brain size of *Mecp2*-mutant animals has been reported to be smaller than that of their WT siblings (Kishi and Macklis 2004), corresponding to smaller cells that are more densely packed (Chen et al. 2001; Kishi and Macklis 2004), we estimated the cell density and width of layer II in the Pir in a DAPI-labelled parallel section of the analysed samples. In addition, we calculated the average diameter of somata of DCX-ir cells. The statistical analyses revealed no significant differences in any of those measures between genotypes, neither in males nor in females (Table 3). Thus, the significant increase in DCX-ir cells in the Pir in *Mecp2*$^{y/-}$ animals is not likely to be due to a brain size effect in our sample.

Similarly to the results in Pir, there was a significant increase of both DCX-ir and DCX-if cells in the Tu of *Mecp2*$^{y/-}$ males with respect to WT (t=-4.65, p=0.001, and t=-2.79, p=0.013) but not in *Mecp2*$^{+/-}$ females with respect to WT (t=-2.00, p=0.08) (Table 2). In sum, we found a significant increase in DCX-expressing cells in olfactory areas in *Mecp2*$^{y/-}$, but not in *Mecp2*$^{+/-}$ animals, as compared with their WT littermates.

The percentage of immature neurons co-expressing DCX/NeuN is differentially affected in olfactory structures in Mecp2$^{y/-}$ male mice

Since our results showed a significant increase in total DCX-expressing cells in olfactory structures in *Mecp2*$^{y/-}$males with respect to their WT controls, we next calculated the percentage of the DCX-if cells that were also expressing NeuN, ie. "transitioning neurons", in the PGl, Pir and Tu in our sample of male mice. Data showed that the percentage of DCX/NeuN-if in the PGl was significantly reduced in *Mecp2*$^{y/-}$males as compared to WT (t=2.49, p=0.03). Thus, although total DCX-if cells were not affected by genotype, the percentage of "transitioning neurons" was reduced in *Mecp2*$^{y/-}$ males. By contrast, the percentages of "transitioning neurons" were not significantly affected by genotype in the Pir or the Tu (t=0.09, p=0.93 and t=2.04, p=0.07, respectively). Regarding the latter result, the total number of double-labelled cells in the Tu was variable, and in fact there were no double-labelled cells in the Tu in 4 out of 10 WT and in 3 out of 8 *Mecp2*$^{y/-}$ mice. The total number of double-labelled DCX/NeuN-if cells in the Tu was not significantly different between genotypes (0.46±0.2 cells/section in the WT vs 0.27±0.12 cells/section in the *Mecp2*$^{y/-}$ mice, p=0.46). Thus, in the OB, where DCX-expressing cells are generated postnatally, lack of MeCP2 did not affect the total DCX-ir cells, but reduced transitioning neurons. However, in the Pir, where, neurons are generated during embryonic development, and in the Tu, lack of MeCP2 increased DCX-cells while not affecting transitioning neurons.

DCX-expressing cells in the striatum and hippocampus are not affected by deficiency of MeCP2

Measures taken in the striatum and hippocampus are summarized in Table 4. Regarding DCX-ir cells in the dorsal striatum, Student's t test revealed no significant differences between *Mecp2*$^{+/-}$ females and their WT controls (t=-1.32, p=0.217) or between *Mecp2*$^{y/-}$ males with respect to WT males (DCX-ir, t=-2.23, p=0.67; DCX-if, t=-0.78, p=0.45). Also, in the ventral striatum, we found no significant differences in females (t=-1.44, p=0.186) or in males (DCX-ir, t=-1.89, p=0.09; DCX-if, t=-0.2, p=0.24). Similarly, percentages of transitioning neurons were not different between *Mecp2*$^{y/-}$ and WT males in the striatum (p>0.5 in both DCX-ir and DCX-if). Finally, in the hippocampus, the Student's t test found no significant differences between genotypes in females (t=-0.72, p=0.49) or in males (t=-0.38, p=0.76). Thus, lack of MeCP2 does not affect the density of DCX-ir cells in the striatum or in the hippocampus.

DISCUSSION

In this study, we analysed the distribution and density of immature, DCX-expressing neurons, in young adult *Mecp2*$^{+/-}$ and *Mecp2*$^{y/-}$ mice, as compared to their WT littermates. Overall, we found no recognizable

qualitative differences in the distribution of DCX-ir somata between WT and mutant mice. On the other hand, and in agreement with a previously suggested role of MeCP2 in neuronal maturation, we found significant increases of DCX-ir cells, immature neurons, in olfactory areas in *Mecp2*$^{y/-}$ males, specifically in the Pir and a newly identified population of DCX cells in the Tu, but not in heterozygous females. In these olfactory areas, the density of double-labelled DCX/NeuN, "transitioning neurons", was not affected by lack of MeCP2. Further, we found no differences in total expression of DCX in the olfactory bulbs, but a decrease in transitioning neurons in the PGl. Finally, density of DCX-ir neurons in the hippocampus and striatum was not affected by deficiency or lack of MeCP2.

The olfactory system provides an excellent model to study neurodevelopmental disorders, and as such it has been studied in both RTT patients and genetically modified mice, with most of the available data obtained in olfactory sensory neurons (OSN) and OB. Thus, early qualitative observations from patient nasal biopsies suggested that a bigger surface area of their nasal epithelium contained olfactory sensory epithelium as compared to healthy controls. In addition, OSN were dysmorphic and increased numbers of immature OSN were found in RTT patients (Ronnett et al. 2003). In *Mecp2*-null mice, there is an early postnatal disorganization in the olfactory epithelium, with more immature OSN at postnatal week 2 and less at postnatal week 7 than in WT (Matarazzo et al. 2004). Two possible hypotheses arise from these data: in a scenario of MeCP2 deficit, 1) there is a deficit in mature OSN leading to a compensatory increase in neurogenesis –at least in the olfactory epithelium, or 2) there is a deficit in terminal differentiation of neurons. Some pieces of evidence support the latter possibility. First, adult neurogenesis experiments showed no differences in incorporation of cells into the olfactory epithelium at postnatal weeks 1, 2 and 7, but only a transient increase at postnatal week 4 (Matarazzo et al. 2004). In addition, although phosphorylation at a specific residue of MeCP2 is key in regulating proliferation and neural differentiation of neural progenitors in culture (Li et al. 2014), proliferation of *Mecp2*-null neural progenitors did not differ from WT *in vitro* or *in vivo* (Smrt et al. 2007). Further, *Mecp2* mutation did not affect the ability of neurospheres derived from *Mecp2*-null or heterozygous mouse embryos to proliferate (Kishi and Macklis 2004). By contrast, a study with mesenchymal cells from 2 patients showed a decrease in cell proliferation, increased senescence markers and reduction of neuronal markers upon an assay of neuronal differentiation (Squillaro et al. 2012). Finally, a study using a mouse model of the *MECP2* duplication syndrome found an increased number of quiescent neural stem cells and neuroblasts

($BrdU^+/DCX^+$) in the dentate gyrus of these mice as compared to WT, but again no differences in proliferation (Chen et al. 2017), suggesting that MeCP2 does not affect proliferation.

Although future experiments studying proliferation should be performed to test for potential undiscovered effects of lack of MeCP2 during embryonic development, a deficit in maturation provoked by lack of MeCP2 is consistent with our data showing increased density of DCX-ir cells at the Pir, in which DCX-ir cells are generated during embryonic development (Rubio et al. 2016), and at the Tu of *Mecp2*$^{y/-}$ mice. However, we did not find significant differences in the DG of the hippocampus, although these post-natally generated cells are also continuously maturing, or in the striatum. Data in the DG are consistent with previously published results showing no differences in total DCX-ir in the hippocampus of a different *Mecp2* KO mouse model (Smrt et al. 2007). In this latter study authors found that the number of "transitioning neurons" was increased in the hippocampus of *Mecp2*-mutant mice, suggesting that immature neurons display a delay in losing DCX expression. Our result in the PGl of the olfactory bulbs, where we found a decrease in "transitioning neurons" in *Mecp2*-null mice, suggests a delay of DCX-expressing cells in acquiring NeuN expression. Both results are in agreement with a dysfunctional maturation process, albeit with different outcome.

There are several possibilities that might explain the region-specific effects of lack of MeCP2. First, the importance of MeCP2 as a regulator and/or the players with which it interacts might be different in each brain area. In fact, a region-specific effect of lack of MeCP2 has been reported in other studies (Santos et al. 2010; Smith et al. 2018). In this framework, the factors regulating maturation differ between embryonic-born cells of the Pir, adult-born cells from the SVZ, and adult-born cells of the DG (Hagg 2005). Consequently, the effect of lack of MeCP2 differs between regions, i.e. it affects density of DCX-expressing cells of embryonic origin and the maturation rate in the postnatally generated cells. We currently do not know whether the small but potentially important population of DCX-ir cells in layer I of the Tu, that was increased in *Mecp2*$^{y/-}$ mice, arise during embryonic development, like Pir cells, or from adult generated progenitors in the SVZ. An embryonic origin is supported by data revealing that protracted neurogenesis in the Tu from progenitors arising from the SVZ and travelling through the ventral migratory stream is restricted to early postnatal days (De Marchis et al. 2004). Second, it is known that stress and corticosterone levels impact the population of DCX-ir in the Pir (Nacher et al. 2004), and those factors are dysregulated in *Mecp2*-mutant animals (McGill et al. 2006; Braun et al. 2012). Third, region-dependent patterns of MeCP2 expression are found in the rodent brain. For example, MeCP2 is

expressed in most (around 60%) neurons in the anterior olfactory nucleus of the rat at birth and remain stable throughout life (Cassel et al. 2004), whereas MeCP2 positive cells in striatum and the DG of the hippocampus appear at reduced numbers (Cassel et al. 2004; Mullaney et al. 2004). Also in the human brain, the dorsal striatum and the hippocampus show weaker staining for MeCP2 (Shahbazian et al. 2002), and these regions displayed no effect of genotype on the total density of DCX-expressing cells (but see the study by Smrt et al. (2007), where they found increased number of "transitioning neurons" in the DG). Finally, putative olfactory deficits due to abnormalities in the olfactory epithelium commented above could influence the rate of maturation in brain olfactory regions. Similarly, structural abnormalities in olfactory structures could cause olfactory impairment, although, to our knowledge, this has not yet been demonstrated in *Mecp2*-null mice, which at least are not anosmic (Moretti et al. 2004).

By contrast to *Mecp2*$^{y/-}$ males, *Mecp2*$^{+/-}$ females did not show any difference in DCX-ir density as compared to their WT controls in our study. Since these females are heterozygous, and therefore they possess a functional *Mecp2* allele, their phenotype is milder than that of the *Mecp2*$^{y/-}$ males (Guy et al. 2001). Still, these females are a valuable model to study the effects of MeCP2 deficiency (Samaco et al. 2013) and their use should not be neglected, especially because RTT affects mainly females. Future studies should be carried out in females of different ages to determine whether some of the effects seen in males may appear at symptomatic stages.

The present study is a promising starting point to investigate the consequences of MeCP2 deficiency in the development and function of the olfactory system and the so-called adult non-proliferative neurogenesis (König et al. 2016). We know that children with autism spectrum disorders, some of which are linked to mutations in *MECP2* (Gonzales and LaSalle 2010), present an aberrant behavioural response to emotional odours, with longer sniff duration for unpleasant odours *versus* pleasant as compared to typically developing children. This aberrant response is correlated with the severity of autistic symptoms (Rozenkrantz et al. 2015). Thus, it would be interesting to test whether increased immature neurons in Pir or Tu might be contributing to some of the aberrant functional responses. Of note, the distribution of DCX-ir cells in the primate (including human) brain is quite more extensive than that shown in rodents, and includes the associative cortices and the amygdala (Liu et al. 2008; Cai et al. 2009; Zhang et al. 2009; Bloch et al. 2011). Given the importance of these structures in cognitive capacities and affective behaviours, a deficient neuronal maturation in these brain areas resulting from the *MECP2* mutations are likely to be involved in the deficits that characterize RTT and autism spectrum disorders.

ETHICAL STANDARDS

The authors declare that they have no conflict of interest. Funded by the Spanish Ministry of Education (BFU2016-77691-C2-1-P) to FMG and EL, Conselleria d'Educació, Investigació, Cultura i Esport (PROMETEO/2016/076) and Universitat Jaume I (UJI-B2016-45) to FMG, Spanish Ministry of Science, Competitiveness and Universities (SAF2015-68436-R) to JN, E-Rare-2 JTC 2012 and E-Rare-2 JTC 2014 by the German Federal Ministry of Education and Research (BMBF) [01GM1302 to M.S., 01GM1505 to O.S.]. Animals were treated throughout according to protocols that were approved by the local veterinary office and carried out in strict accordance with EU directive 2010/63/EU and the German law.

REFERENCES

Amir RE, Van den Veyver IB, Wan M, et al (1999) Rett syndrome is caused by mutations in X-linked MECP2, encoding methyl- CpG-binding protein 2. Nat Genet 23:185–188. doi: 10.1038/13810

Bloch J, Kaeser M, Sadeghi Y, et al (2011) Doublecortin-positive cells in the adult primate cerebral cortex and possible role in brain plasticity and development. J Comp Neurol. doi: 10.1002/cne.22547

Braun S, Kottwitz D, Nuber UA (2012) Pharmacological interference with the glucocorticoid system influences symptoms and lifespan in a mouse model of Rett syndrome. Hum Mol Genet 21:1673–1680. doi: 10.1093/hmg/ddr602

Cai Y, Xiong K, Chu Y, et al (2009) Doublecortin expression in adult cat and primate cerebral cortex relates to immature neurons that develop into GABAergic subgroups. Exp Neurol. doi: 10.1016/j.expneurol.2008.12.008

Cassel S, Revel MO, Kelche C, Zwiller J (2004) Expression of the methyl-CpG-binding protein MeCP2 in rat brain. An ontogenetic study. Neurobiol Dis 15:206–211. doi: 10.1016/j.nbd.2003.10.011

Chen RZ, Akbarian S, Tudor M, Jaenisch R (2001) Deficiency of methyl-CpG binding protein-2 in CNS neurons results in a Rett-like phenotype in mice. Nat Genet 27:327–331. doi: 10.1038/85906

Chen Z, Li X, Zhou J, et al (2017) Accumulated quiescent neural stem cells in adult hippocampus of the mouse model for the MECP2 duplication syndrome. Sci Rep 7:41701. doi: 10.1038/srep41701

Cohen DRS, Matarazzo V, Palmer AM, et al (2003) Expression of MeCP2 in olfactory receptor neurons is developmentally regulated and occurs before synaptogenesis. Mol Cell Neurosci 22:417–29. doi:

10.1016/S1044-7431(03)00026-5

De Marchis S, Fasolo A, Puche AC (2004) Subventricular zone-derived neuronal progenitors migrate into the subcortical forebrain to postnatal mice. J Comp Neurol 476:290–300. doi: 10.1002/cne.20217

Francis F, Koulakoff A, Boucher D, et al (1999) Doublecortin is a developmentally regulated, microtubule-associated protein expressed in migrating and differentiating neurons. Neuron 23:247–256. doi: 10.1016/S0896-6273(00)80777-1

Gleeson JG, Allen KM, Fox JW, et al (1998) doublecortin, a brain-specific gene mutated in human X-linked lissencephaly and double cortex syndrome, encodes a putative signaling protein. Cell 92:63–72. doi: 10.1016/S0092-8674(00)80899-5

Gómez-Climent Á, Hernández-González S, Shionoya K, et al (2011) Olfactory bulbectomy, but not odor conditioned aversion, induces the differentiation of immature neurons in the adult rat piriform cortex. Neuroscience. doi: 10.1016/j.neuroscience.2011.03.004

Gómez-Climent MÁ, Castillo-Gómez E, Varea E, et al (2008) A population of prenatally generated cells in the rat paleocortex maintains an immature neuronal phenotype into adulthood. Cereb Cortex 18:2229–2240. doi: 10.1093/cercor/bhm255

Gonzales ML, LaSalle JM (2010) The role of MeCP2 in brain development and neurodevelopmental disorders. Curr. Psychiatry Rep. 12:127–134

Guillemot F, Molnár Z, Tarabykin V, Stoykova A (2006) Molecular mechanisms of cortical differentiation. Eur. J. Neurosci.

Guy J, Hendrich B, Holmes M, et al (2001) A mouse Mecp2-null mutation causes neurological symptoms that mimic Rett syndrome. Nat Genet 27:322–6. doi: 10.1038/85899

Hagberg B (2002) Clinical manifestations and stages of Rett syndrome. Ment Retard Dev Disabil Res Rev 8:61–65. doi: 10.1002/mrdd.10020

Hagg T (2005) Molecular regulation of adult CNS neurogenesis: An integrated view. Trends Neurosci.

Kishi N, Macklis JD (2004) MECP2 is progressively expressed in post-migratory neurons and is involved in neuronal maturation rather than cell fate decisions. Mol Cell Neurosci 27:306–321. doi: 10.1016/j.mcn.2004.07.006

König R, Benedetti B, Rotheneichner P, et al (2016) Distribution and fate of DCX/PSA-NCAM expressing cells in the adult mammalian cortex: A local reservoir for adult cortical neuroplasticity? Front. Biol. (Beijing).

Li H, Zhong X, Chau KF, et al (2014) Cell cycle-linked MeCP2 phosphorylation modulates adult neurogenesis involving the Notch signalling pathway. Nat Commun 5:5601. doi: 10.1038/ncomms6601

Liu YWJ, Curtis MA, Gibbons HM, et al (2008) Doublecortin expression in the normal and epileptic adult human brain. Eur J Neurosci. doi: 10.1111/j.1460-9568.2008.06518.x

Lombardi LM, Baker SA, Zoghbi HY (2015) MECP2 disorders: From the clinic to mice and back. J. Clin. Invest. 125:2914–2923

Luzzati F, Bonfanti L, Fasolo A, Peretto P (2009) DCX and PSA-NCAM Expression identifies a population of neurons preferentially distributed in associative areas of different pallial derivatives and vertebrate species. Cereb Cortex. doi: 10.1093/cercor/bhn145

Matarazzo V, Cohen D, Palmer AM, et al (2004) The transcriptional repressor Mecp2 regulates terminal neuronal differentiation. Mol Cell Neurosci 27:44–58. doi: 10.1016/j.mcn.2004.05.005

McGill BE, Bundle SF, Yaylaoglu MB, et al (2006) Enhanced anxiety and stress-induced corticosterone release are associated with increased Crh expression in a mouse model of Rett syndrome. Proc Natl Acad Sci. doi: 10.1073/pnas.0608702103

Moretti P, Bouwknecht JA, Teague R, et al (2004) Abnormalities of social interactions and home cage behavior in a mouse model of Rett syndrome. Hum Mol Genet

Mullaney BC, Johnston M V., Blue ME (2004) Developmental expression of methyl-CpG binding protein 2 is dynamically regulated in the rodent brain. Neuroscience 123:939–949. doi: 10.1016/j.neuroscience.2003.11.025

Nacher J, Crespo C, McEwen BS (2002) Doublecortin expression in the adult rat telencephalon. Eur J Neurosci 14:629–644. doi: 10.1046/j.0953-816X.2001.01683.x

Nacher J, Pham K, Gil-Fernandez V, Mcewen BS (2004) Chronic restraint stress and chronic corticosterone treatment modulate differentially the expression of molecules related to structural

plasticity in the adult rat piriform cortex. Neuroscience. doi: 10.1016/j.neuroscience.2004.03.038

Nan X, Campoy FJ, Bird A (1997) MeCP2 is a transcriptional repressor with abundant binding sites in genomic chromatin. Cell 88:471–481. doi: 10.1016/S0092-8674(00)81887-5

Nan X, Meehan RR, Bird A (1993) Dissection of the methyl-CpG binding domain from the chromosomal protein MeCP2. Nucleic Acids Res 21:4886–4892. doi: 10.1093/nar/21.21.4886

Paxinos G, Franklin K (2012) Paxinos and Franklin's the Mouse Brain in Stereotaxic Coordinates. In: Acad. Press. https://www.elsevier.com/books/paxinos-and-franklins-the-mouse-brain-in-stereotaxic-coordinates/paxinos/978-0-12-391057-8

Ronnett G V., Leopold D, Cai X, et al (2003) Olfactory biopsies demonstrate a defect in neuronal development in Rett's syndrome. Ann Neurol 54:206–18. doi: 10.1002/ana.10633

Rotheneichner P, Belles M, Benedetti B, et al (2018) Cellular Plasticity in the Adult Murine Piriform Cortex: Continuous Maturation of Dormant Precursors Into Excitatory Neurons. Cereb Cortex. doi: 10.1093/cercor/bhy087

Rozenkrantz L, Zachor D, Heller I, et al (2015) A Mechanistic Link between Olfaction and Autism Spectrum Disorder. Curr Biol 25:1904–1910. doi: 10.1016/j.cub.2015.05.048

Rubio A, Belles M, Belenguer G, et al (2016) Characterization and isolation of immature neurons of the adult mouse piriform cortex. Dev Neurobiol 76:748–763. doi: 10.1002/dneu.22357

Saaltink D-J, Håvik B, Verissimo CS, et al (2012) Doublecortin and doublecortin-like are expressed in overlapping and non-overlapping neuronal cell population: implications for neurogenesis. J Comp Neurol 520:2805–23. doi: 10.1002/cne.23144

Samaco RC, Mcgraw CM, Ward CS, et al (2013) Female Mecp2+/- mice display robust behavioral deficits on two different genetic backgrounds providing a framework for pre-clinical studies. Hum Mol Genet 22:96–109. doi: 10.1093/hmg/dds406

Santos M, Summavielle T, Teixeira-Castro A, et al (2010) Monoamine deficits in the brain of methyl-CpG binding protein 2 null mice suggest the involvement of the cerebral cortex in early stages of Rett syndrome. Neuroscience. doi: 10.1016/j.neuroscience.2010.07.010

Santos M, Temudo T, Kay T, et al (2009) Mutations in the MECP2 gene are not a major cause of Rett

syndrome-like or related neurodevelopmental phenotype in male patients. J Child Neurol 24:49–55

Shahbazian MD, Antalffy B, Armstrong DL, Zoghbi HY (2002) Insight into Rett syndrome: MeCP2 levels display tissue- and cell-specific differences and correlate with neuronal maturation. Hum Mol Genet 11:115–24. doi: 10.1093/hmg/11.2.115

Smith ES, Smith DR, Eyring C, et al (2018) Altered trajectories of neurodevelopment and behavior in mouse models of Rett syndrome. Neurobiol Learn Mem Epub ahead: doi: 10.1016/j.nlm.2018.11.007

Smrt RD, Eaves-Egenes J, Barkho BZ, et al (2007) Mecp2 deficiency leads to delayed maturation and altered gene expression in hippocampal neurons. Neurobiol Dis 27:77–89. doi: 10.1016/j.nbd.2007.04.005

Squillaro T, Alessio N, Cipollaro M, et al (2012) Reduced expression of MECP2 affects cell commitment and maintenance in neurons by triggering senescence: new perspective for Rett syndrome. Mol Biol Cell 23:1435–1445. doi: 10.1091/mbc.E11-09-0784

Zhang X-M, Cai Y, Chu Y, et al (2009) Doublecortin-expressing cells persist in the associative cerebral cortex and amygdala in aged nonhuman primates. Front Neuroanat. doi: 10.3389/neuro.05.017.2009

FIGURE LEGENDS

Figure 1. Representative microphotographs of the distribution of DCX-ir in the brain of *Mecp2*-mutant and WT mice. A) Example of DCX-ir in the SVZ and dSt (inset) in a WT female. B) DCX-ir in the ventral part of the SVZ and vST in a WT male. B') DCX-ir in the vSt of a *Mecp2*$^{y/-}$ male. C) DCX-ir in the DG of a WT female. No significant differences were found in the density of DCX-ir somata between genotypes in any of the sexes. D) DCX-ir in the OB of a WT male. D') DCX-ir in the OB of a *Mecp2*$^{y/-}$ male. Although the apparent intensity of the immunostaining seems higher than in the WT male specimen, the area fraction occupied by DCX-ir was not significantly higher in the mutant animals. E) DCX-ir in the Pir of a WT male. E') DCX-ir in the Pir of *Mecp2*$^{y/-}$ male. The average density of DCX-ir somata was significantly increased in layer II of the Pir in *Mecp2*$^{y/-}$ males as compared to WT. F) DCX-ir in layer I of Tu on a WT male. F') DCX-ir in layer I of Tu on *Mecp2*$^{y/-}$ males, which was significantly increased as compared to WT. Scale bar: 100 μm. aca: anterior commisure; AcbC: core of the nucleus accumbens; AOB: accessory olfactory bulb; AOL: anterior olfactory nucleus, lateral; AOM: anterior olfactory nucleus, medial; AOV: anterior olfactory nucleus, ventral; CC: corpus callosum; CPu: caudatus putamen; DG: dentate gyrus of the hippocampus; Gl: glomerular cell layer of the olfactory bulb; Gr: granular layer of the olfactory bulb; GrDG: granular layer of the dentate gyrus; LV: lateral ventricle; Mi: mitral cell layer of the olfactory bulb; Mol: molecular layer of the dentate gyrus; PoDG: Polymorphic-oriens layer of the dentate gyrus; Pir: piriform cortex; Tu: olfactory tubercle.

Figure 2. Representative images of regions of the olfactory system of *Mecp2*$^{y/-}$ and WT male mice co-labelled by immunofluorescence for DCX (red) and NeuN (green). A) Example of DCX-if fibres and somata (inset) found in the olfactory bulb of a WT male. B) Olfactory bulb of a WT male, showing an example of a transitioning neuron in the periglomerular zone co-labelled for DCX and NeuN in the inset. C) Example of DCX-if in the piriform cortex of a *Mecp2*$^{y/-}$, showing a DCX^{+}/NeuN^{-} cell in the inset. D) Olfactory tubercle from a *Mecp2*$^{y/-}$ male showing a cluster of DCX-if cells in layer I. Three "transitioning cells", immature neurons co-labelled by DCX and NeuN, and four DCX^{+}/NeuN^{-} cells are displayed in the inset. Scale bar 100μm, in insets 10μm.

Table 1. Bregma levels selected for quantification of DCX-ir and DCX/NeuN-if cells in the different brain nuclei analysed.

Nucleus	Approximate mm to Bregma
Olfactory bulbs	+3.2, +3.1, +3
Dorsal Striatum	+1.5, +1.1, +0.7
Ventral Striatum	+1.5, +1.1, +0.7
Olfactory tubercle	+1.7, +1.5, +1.3, +1.1
Piriform cortex	+1, 0, -1, -2
Hippocampus	-1.4, -2.2, -2.8, -3.2

Table 2. Quantitative analysis of DCX-ir, DCX-if and double DCX/NeuN-if cell density in the olfactory system of wild-type and *Mecp2*-deficient mice. Significant differences between genotypes are highlighted in bold **, p<0.01; ***p<0.001 *Mecp2* vs WT.

			DCX-ir (DAB)	DCX-if	DCX/NeuN-if
OB, Gr	Females	WT	a.f. 18.94±1.94		
		Mecp2$^{+/-}$	a.f. 23.52±3.80		
	Males	WT	a.f. 20.21±3.21	o.d. 0.139±0.003	
		Mecp2$^{y/-}$	a.f. 28.13±1.51	o.d 0.148±0.003	
OB, PGl	Males	WT		28.89 cells/mm^2±4.21	**4.96%±1.69**
		Mecp2$^{y/-}$		33.85 cells/mm2±3.23	**1.09%±0.71****
Pir	Females	WT	26.0 cells/mm2±2.8		
		Mecp2$^{+/-}$	29.1 cells/mm2±2.5		
	Males	WT	**24.2 cells/mm2±2.5**	**30.6 cells/mm2±2.7**	29.3%±4.7
		Mecp2$^{y/-}$	**44.2 cells/mm^2±4.4*****	**43.9 cells/mm2±4.1****	28.7%±4.4
Tu	Females	WT	0.6 cells/section±0.2		
		Mecp2$^{+/-}$	2.9 cells/section ±1.0		
	Males	WT	**2.3 cells/section±0.4**	**6.17 cells/section±1.8**	7.1%±2.2
		Mecp2$^{y/-}$	**6.6 cells/section ±1.0*****	**14.0 cells/section±2.2****	2.1%±0.9

Values are presented as mean ± SEM

Table 3. Quantitative analysis of cell density, width of layer II and diameter of DCX-ir somata in the piriform cortex of wild-type and *Mecp2*-deficient mice.

Cell density (average of both hemispheres, nuclei/mm^2)	Females	WT	2826.3±108.0	p=0.66
		Mecp2$^{+/-}$	2899.0±116.6	
	Males	WT	2464.7±56.9	p=0.56
		Mecp2$^{y/-}$	2514.4±57.5	
Width of layer II (average, µm)	Females	WT	128.7±8,2	p=0.38
		Mecp2$^{+/-}$	121.2±4.8	
	Males	WT	129.6±2.9	p=0.87
		Mecp2$^{y/-}$	128.8±3.8	
Diameter of the soma (average, µm)	Females	WT	12.2±0.3	p=0.21
		Mecp2$^{+/-}$	11.6±0.2	
	Males	WT	11.7±0.1	p=0.68
		Mecp2$^{y/-}$	11.9±0.4	

Values are presented as mean ± SEM

Table 4. Quantitative analysis of DCX-ir, DCX-if and double DCX/NeuN-if cell density in the striatum and hippocampus of wild-type and *Mecp2*-deficient mice.

			DCX-ir (DAB)	DCX-if	DCX/NeuN-if
dSt	Females	WT	21.7 cells/mm^2±2.5		
		Mecp2$^{+/-}$	27.0 cells/mm^2±3.0		
	Males	WT	39.9 cells/mm^2±6.0	28.6 cells/mm^2±2.6	14.4%±4.1
		Mecp2$^{y/-}$	48.8 cells/mm^2±5.3	33.3 cells/mm^2±6.3	14.7%±4.7
vSt	Females	WT	56.0 cells/mm^2±4.7		
		Mecp2$^{+/-}$	64.2 cells/mm^2±2.9		
	Males	WT	81.7 cells/mm^2±9.8	106.5 cells/mm^2±5.9	4.7%±1.8
		Mecp2$^{y/-}$	110.0 cells/mm^2±12.2	121.2 cells/mm^2±12.3	6.0%±2.0
DG	Females	WT	354.8 cells/section ±20.0		
		Mecp2$^{+/-}$	376.8 cells/section±15.8		
	Males	WT	386.6 cells/section ±23.4		
		Mecp2$^{y/-}$	398.7 cells/section ±29.1		

Values are presented as mean ± SEM

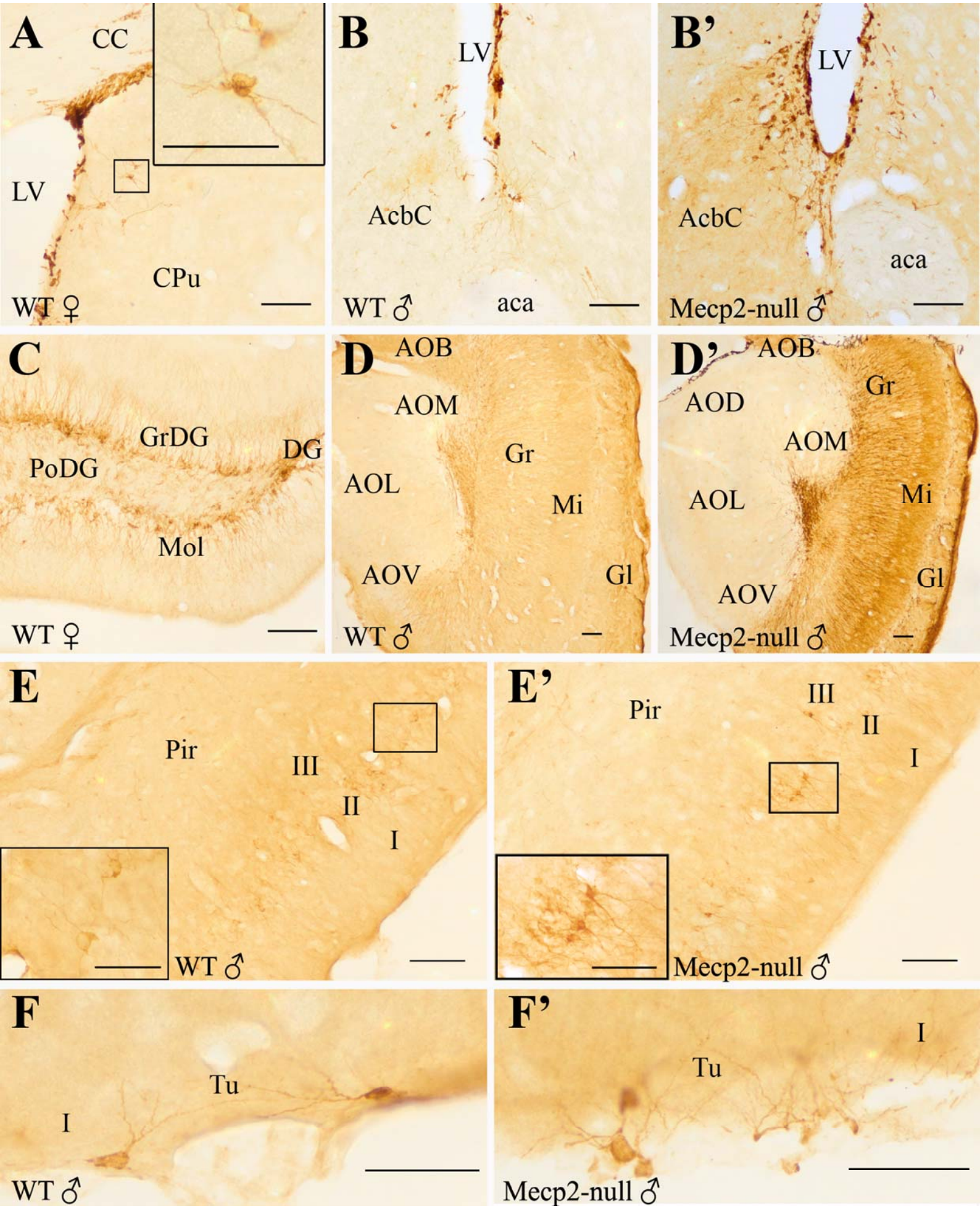
A
CC
LV
CPu
WT ♀
B
LV
AcbC
WT ♂
aca
B'
LV
AcbC
aca
Mecp2-null ♂
C
GrDG
DG
PoDG
Mol
WT ♀
D
AOB
AOM
Gr
AOL
Mi
AOV
Gl
WT ♂
D'
AOB
Gr
AOD
AOM
AOL
Mi
AOV
Gl
Mecp2-null ♂
E
Pir
III
II
I
WT ♂
E'
Pir
III
II
I
Mecp2-null ♂
F
Tu
I
WT ♂
F'
I
Tu
Mecp2-null ♂

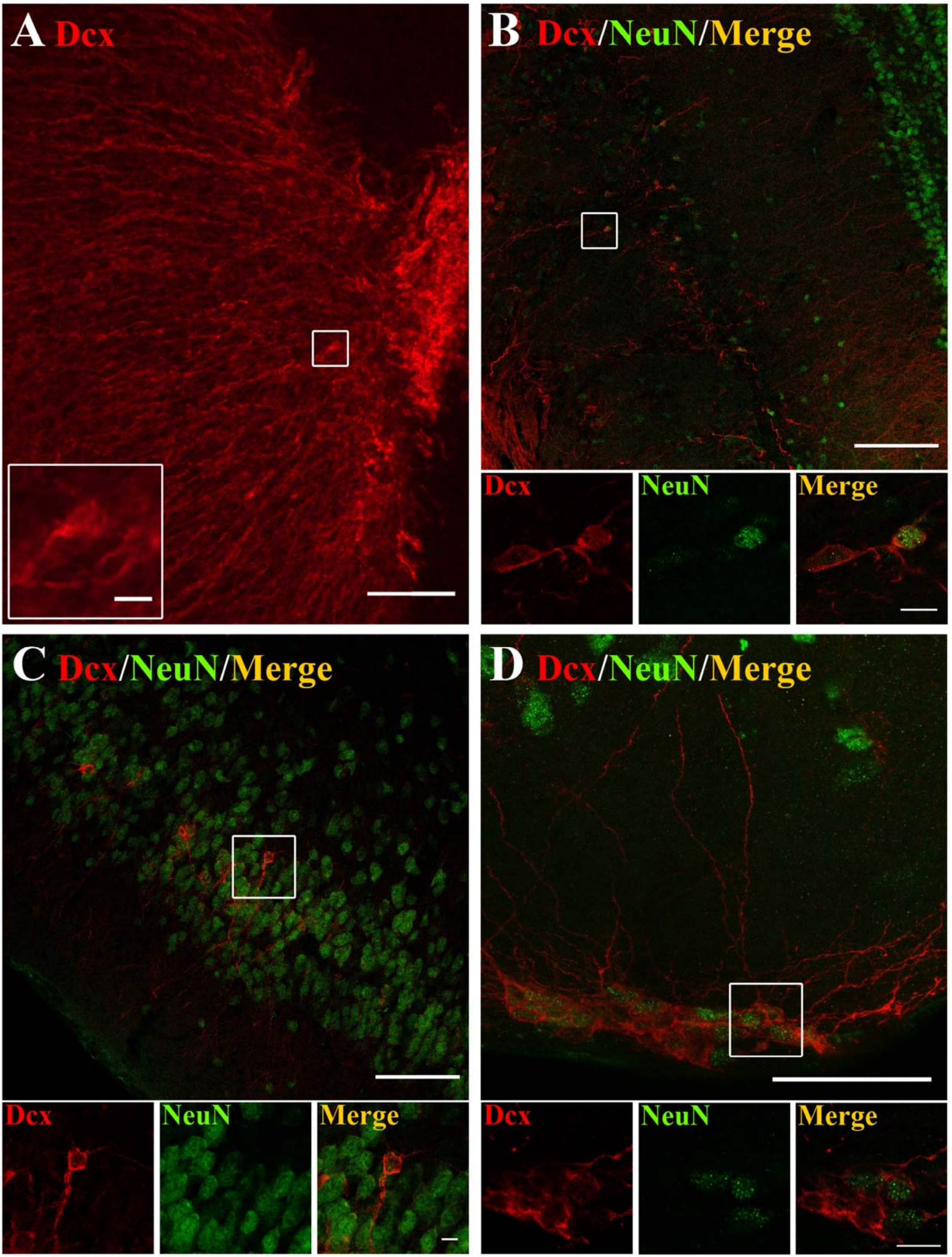
A Dcx
B Dcx/NeuN/Merge
Dcx
NeuN
Merge
C Dcx/NeuN/Merge
D Dcx/NeuN/Merge
Dcx
NeuN
Merge
Dcx
NeuN
Merge

SUPPLEMENTARY INFORMATION

TITLE: Lack of MeCP2 leads to region-specific increase of doublecortin in the olfactory system

AUTHORS: Elena Martínez-Rodríguez[1], Ana Martín-Sánchez[2§], Simona Coviello[3], Cristina Foiani[1], Emre Kul[4], Oliver Stork[4], Fernando Martínez-García[2], Juan Nacher[3], Enrique Lanuza[1], Mónica Santos[3*], Carmen Agustín-Pavón[1*]

1. Unitat Mixta d'Investigació Neuroanatomia Funcional, Departament de Biologia Cel·lular, Funcional i Antropologia Física, Universitat de València (Spain).

2. Unitat Mixta d'Investigació Neuroanatomia Funcional, Unitat Predepartamental de Medicina, Universitat Jaume I, Castelló (Spain).

3. Neurobiology Unit, Department of Cell Biology, Interdisciplinary Research Structure for Biotechnology and Biomedicine (BIOTECMED), Universitat de Valencia (Spain); CIBERSAM: Spanish National Network for Research in Mental Health (Spain); Fundación Investigación Hospital Clínico de Valencia, INCLIVA, Valencia (Spain).

4. Institute of Biology, Otto-von-Guericke University, Magdeburg (Germany)

§ Current adress: Departament de Ciències Experimentals i de la Salut, Grup de Recerca en Neurobiologia del Comportament (GReNeC-NeuroBio), Institut Hospital del Mar d'Investigacions Mèdiques (IMIM), Universitat Pompeu Fabra, Barcelona (Spain)

SUPPLEMENTARY METHODS

To confirm the presence of DCX-expressing cells in the Tu of another strain of mice, and further characterize these cells, we used eight 3 months-old male mice from the strain FVB obtained from Jackson laboratories (Bar Harbor, Maine, USA). The animal room was maintained under controlled conditions of temperature (25 °C) and humidity (50%) on a reverse light/dark cycle (lights on at 23:00 and lights off at 11:00).

Mice were perfused transcardially under deep pentobarbital anaesthesia (0.01mL/g in 0.9% NaCl solution, Sigma Aldrich) first for 1 min with saline and then for 30 min with 4% paraformaldehyde in sodium phosphate buffer (PB) 0.1 M, pH 7.4. Thirty minutes after perfusion, brains were extracted from the skull and sectioned with a vibratome (Leica VT 1000E, Leica) and 50-µm- thick coronal sections were collected in 6 sequential subseries and kept in cold PB (4°C) until used.

We performed a triple immunodetection of DCX, the polysialylated form of the neural cell adhesion molecule (PSA-NCAM), a plasticity marker found in immature neurons; and neuronal nuclear antigene (NeuN), a neuronal marker. In brief, for anti-PSA-NCAM staining, an antigen retrieval step was performed, consisting in a pretreatment with sodium citrate buffer (10 Mm, pH 6.0) for 1 min at 100 ºC. After cooling down the sections to room temperature, they were incubated "free-floating" in 10% normal donkey serum (NDS; AbCys) for 1hour at RT to block inespecific sites of bindings. Then, slices were incubated for two nights at 4 ºC with a mix of primary antibodies: Rabbit IgG anti-DCX (1:1000; Abcam), Mouse IgM anti PSA-NCAM (1:1400, Millipore) and Mouse IgG_1 anti-NeuN (1:500, Millipore) with 5% NDS and 0.3% Triton-X100. The next day, after rinsing with PBS sections were incubated for one hour at RT with: Goat anti-Rabbit IgG A555, Goat anti-Mouse IgM A488, and Goat anti-Mouse IgG_1 A647 (1:400, Invitrogen) secondary antibodies. Finally, sections were mounted on slides and covered using Fluorescence Mounting Medium (Dako Omnis).

Sections processed for fluorescent immunohistochemistry were observed under a confocal microscope using a 20x objective (Leica, TCS-SPE). Different coronal sections containing tubercle (Tu) were selected per animal between Bregma -1.70 mm to 0.74 mm. Then Z-series of optical sections (1µm step size) covering all its three-dimensional extension were acquired using sequential scanning mode with 2.5x-digital zoom.

Immunolabelled neurons in the olfactory tubercle (Tu) were quantified by opening the confocal images with ImageJ and counting in the composite images with the multipoint tool and the help of the multichannel tool the single DCX-if, double DCX/PSA-NCAM-if and triple DCX/PSA-NCAM/NeuN-if cells.

SUPPLEMENTARY TABLE

Summary of DCX-if cells sampled in the Tu of male mice, and percentages of these cells that expressed DCX only, co-expressed PSA-NCAM, co-expressed both PSA-NCAM and NeuN, or co-expressed NeuN only. Data show that most DCX-if cells were also PSA-NCAM-if, and some of them co-expressed the neuronal marker NeuN, supporting the idea that these cells found in layer I of the Tu are immature neurons.

DCX-if cells	**$DCX^+/PSA\text{-}NCAM^-/NeuN^-$**	**$DCX^+/PSA\text{-}NCAM^+/NeuN^-$**	**$DCX^+/PSA\text{-}NCAM^+/NeuN^+$**	**$DCX^+/PSA\text{-}NCAM^+$ both $NeuN^-$ and $NeuN^+$**	**$DCX^+/PSA\text{-}NCAM^-/NeuN^+$**
5.3±1.2 cells/section	18.96%±6.58	52.81%±11.18	26.67±14.49%	79.48±6.54%	1.56±1.56%

SUPPLEMENTARY FIGURE

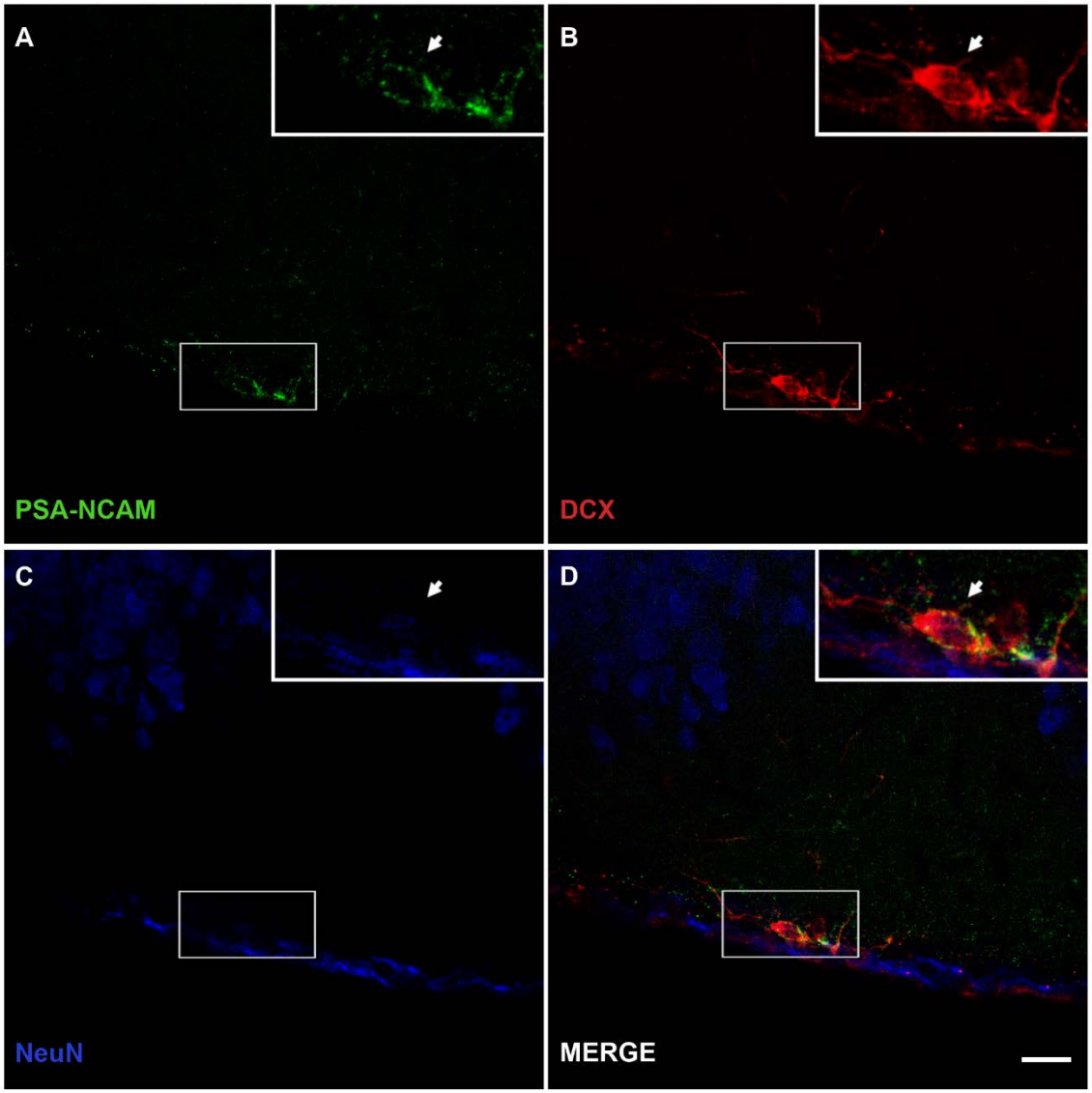

Fig S1. Confocal microscopic analysis of the phenotype of immature cells in the olfactory tubercle (Tu). Triple PSA-NCAM/DCX/NeuN immunofluorescence. Single confocal planes showing the expression of PSA-NCAM (A), DCX (B) and NeuN (C) and merge (D) in WT mice. Scale bars: 20 µm; for inserts: 10µm. PSA-NCAM: polysialylated form of the neural cell adhesion molecule; DCX: doublecortin; NeuN: neuronal nuclear antigene.